Systematics of ground-state quadrupole moments of odd-A deformed nuclei determined with muonic M x rays

Y. Tanaka and R. M. Steffen
Department of Physics, Purdue University, West Lafayette, Indiana 47907

E. B. Shera, W. Reuter, and M. V. Hoehn
Los Alamos National Laboratory, Los Alamos, New Mexico 87545

J. D. Zumbro
Department of Physics, Princeton University, Princeton, New Jersey 08544

(Received 15 November 1983)

The ground-state quadrupole moments of ^{151}Eu, ^{153}Eu, ^{159}Tb, ^{163}Dy, ^{167}Er, ^{177}Hf, ^{179}Hf, ^{191}Ir, and ^{193}Ir were determined by measuring the quadrupole hyperfine-splitting energies of muonic M x rays. The results are $Q=0.903(10)$ e b for ^{151}Eu, $Q=2.412(21)$ e b for ^{153}Eu, $Q=1.432(8)$ e b for ^{159}Tb, $Q=2.648(21)$ e b for ^{163}Dy, $Q=3.565(29)$ e b for ^{167}Er, $Q=3.365(29)$ e b for ^{177}Hf, $Q=3.793(33)$ e b for ^{179}Hf, $Q=0.816(9)$ e b for ^{191}Ir, and $Q=0.751(9)$ e b for ^{193}Ir. The present quadrupole moments, compared with values obtained from electronic-atom hyperfine measurements, show that the Sternheimer correction factors used in the rare-earth electronic-atom analysis are unreliable. Systematics of deformation parameters β_2 calculated from the present quadrupole moments for odd-A nuclei, and from $B(E2)$ values of Coulomb excitation measurements for even-A nuclei, also indicate that the largest deformation change so far known exists between ^{151}Eu and ^{153}Eu. Except at the onset of nuclear deformation, the deformation parameters of the odd-A nuclei are quite consistent with those of the even-A neighbors.

I. INTRODUCTION

Precise measurements of nuclear quadrupole moments have been hindered by the fact that no external electrostatic field gradient is strong enough to produce observable hyperfine energy splittings. One must therefore rely on the electrostatic field gradient of the atomic environment of the nucleus. The field gradient produced by electrons is difficult to compute precisely in a multielectron system, and hence electronic-atom hyperfine experiments, although very precise with respect to energy splittings, often yield unreliable values for extracted nuclear quadrupole moments.

In muonic atoms, on the other hand, the electrostatic field gradient at the nucleus is produced by a single muon (the electronic contribution is negligibly small) and can be precisely calculated. Furthermore, muonic $3d$ orbits in heavy atoms are close enough to the nucleus to produce large hyperfine splittings, yet far enough from the nucleus to avoid any serious model dependence caused by the finite size of the nuclear charge distribution.[1-7]

Ground-state quadrupole moments deduced from the muonic M x-ray analysis can be used in combination with electronic-atom measurements to calibrate the electronic field gradient at the nucleus. Once the electronic field gradient is known for a particular element, electronic-atom experiments can yield accurate quadrupole-moment values for a wide range of isotopes of the same Z. The implication of the present work toward understanding the electrostatic field gradient in rare-earth atoms, including extraction of experimental values for the Sternheimer factor, was the subject of a previous publication.[8] The present paper presents the details of the experiments, the method of extracting the quadrupole moments, and a discussion of the systematics of nuclear quadrupole deformation in the rare-earth region, with emphasis on odd-A nuclei.

II. THE QUADRUPOLE HYPERFINE INTERACTION IN MUONIC ATOMS

The matrix elements of the electric quadrupole hyperfine interaction are given[9] by

$$\langle I'j';F\,|\,H_{E2}\,|\,Ij;F\rangle=-e^2(-1)^{I+j+F}\frac{\sqrt{4\pi(2j'+1)}}{\sqrt{5}}\begin{Bmatrix} I & j & F \\ j' & I' & 2\end{Bmatrix}(j'\tfrac{1}{2}20\,|\,j\tfrac{1}{2})W_{E2}^{I'j'Ij}\ , \tag{1}$$

where I and j specify nuclear and muonic states, respectively, and F denotes the total angular momentum of the coupled muon-nuclear states. The last factor in Eq. (1) is the radial integral of the quadrupole interaction,

$$W_{E2}^{I'j'Ij}=\int \rho_{E2}^{I'I}(r)V_{E2}^{j'j}(r)r^2dr\ , \tag{2}$$

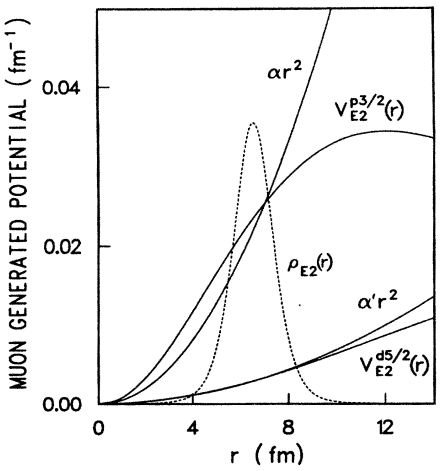

FIG. 1. Muon generated quadrupole potentials $V_{E2}(r)$ and the corresponding point nucleus potentials αr^2 with $\alpha=\langle j' \mid 1/r_\mu^3 \mid j \rangle$ of Eq. (6). A quadrupole transition charge density in arbitrary units is also displayed by the dotted curve.

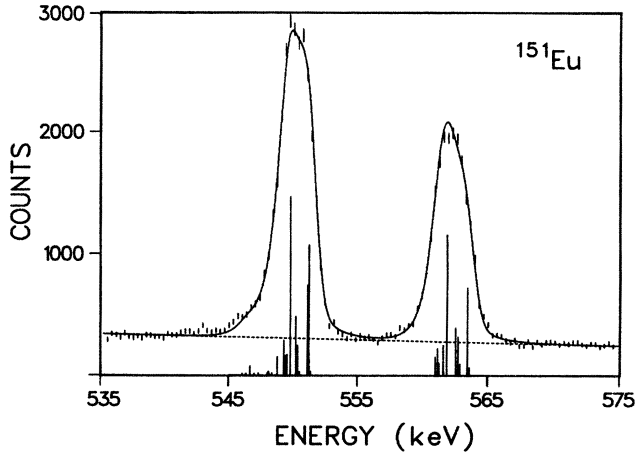

FIG. 3. The muonic M x-ray spectrum of ^{151}Eu. The solid curve represents the best-fit spectrum computed from theory. The vertical lines show the calculated transition energies and intensities. The deduced ground-state quadrupole moment is $Q(\frac{5}{2}^+)=0.903(10)\ e$ b.

which describes the overlap of the nuclear quadrupole charge density

$$\rho_{E2}(r)=\int \rho(r,\theta,\phi)Y_{20}(\theta,\phi)d\Omega \tag{3}$$

with the muon-generated quadrupole potential

$$V_{E2}^{j'j}(r)=\int \frac{r_<^2}{r_>^3}(G_{j'}G_j+F_{j'}F_j)dr_\mu \ . \tag{4}$$

Here G_j and F_j are radial wave functions of a muon in the angular momentum state j, and $r_>$ ($r_<$) takes the larger (smaller) of the muon and nuclear coordinates r_μ and r.

The quadrupole charge density of Eq. (3) can be derived from a deformed Fermi distribution:

$$\rho(r,\theta,\phi)=\rho_0\Big/\left[1+\exp\left[\frac{r-R(\theta,\phi)}{a}\right]\right], \tag{5a}$$

with

$$R(\theta,\phi)=R_Q[1+\beta_2 Y_{20}(\theta,\phi)] \ . \tag{5b}$$

In this approximation the quadrupole charge density is peaked near the nuclear surface as shown in Fig. 1, and the radial position of the peak is approximately given by the value of R_Q.

If the muon is sufficiently far away from the nucleus, one can assume that the probability is negligible of finding

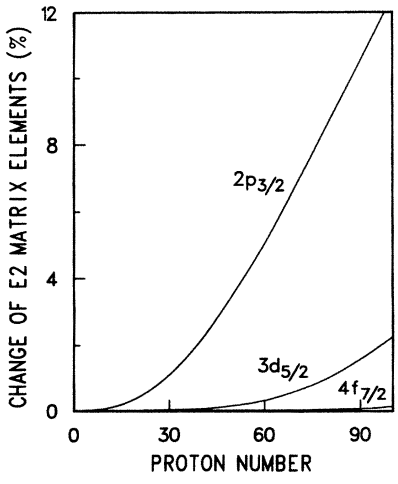

FIG. 2. Change of deduced $E2$ matrix elements caused by a 10% change of the quadrupole charge radius R_Q of the transition charge density $\rho_{E2}(r)$.

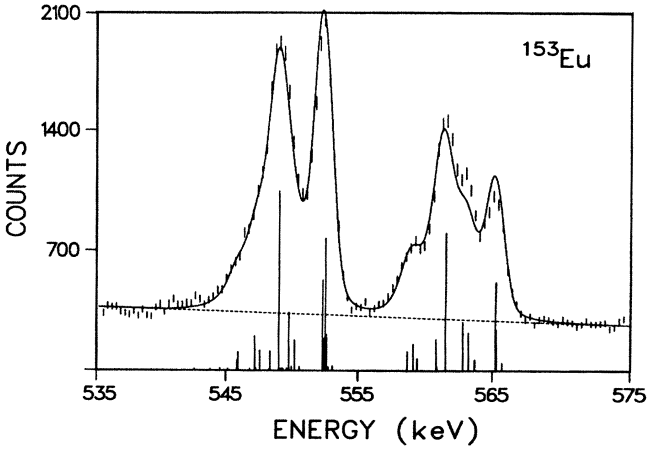

FIG. 4. The muonic M x-ray spectrum of ^{153}Eu. The solid curve represents the best-fit spectrum computed from theory. The vertical lines show the calculated transition energies and intensities. The deduced ground-state quadrupole moment is $Q(\frac{5}{2}^+)=2.412(21)\ e$ b.

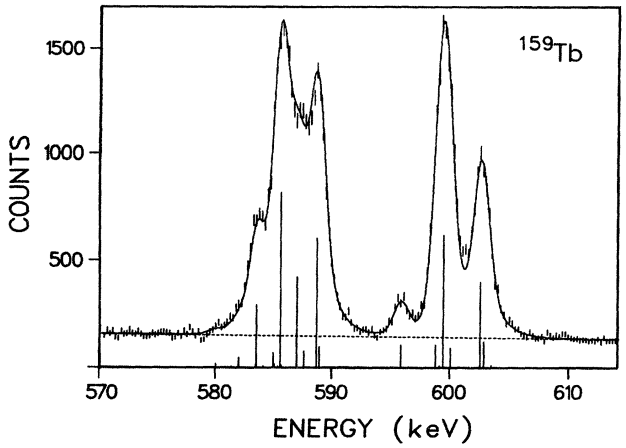

FIG. 5. The muonic M x-ray spectrum of ^{159}Tb. The solid curve represents the best-fit spectrum computed from theory. The vertical lines show the calculated transition energies and intensities. The deduced ground-state quadrupole moment is $Q(\frac{3}{2}^+)=1.432(8)\ e$ b.

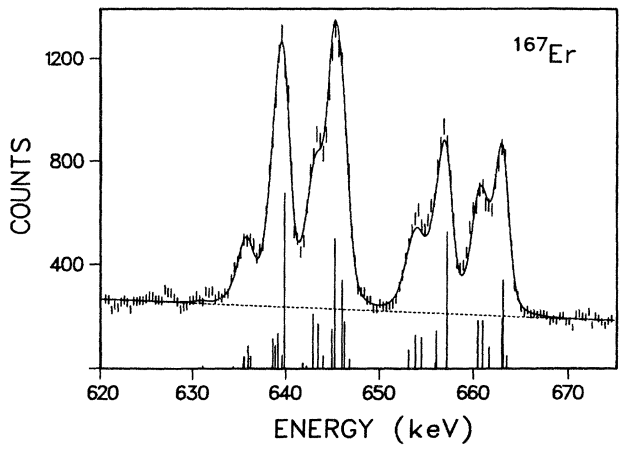

FIG. 7. The muonic M x-ray spectrum of ^{167}Er. The solid curve represents the best-fit spectrum computed from theory. The vertical lines show the calculated transition energies and intensities. The deduced ground-state quadrupole moment is $Q(\frac{7}{2}^+)=3.565(29)\ e$ b.

the muon inside the nucleus. The muon-generated quadrupole potential then reduces to

$$V_{E2}^{j'j}(r)=r^2\left\langle j'\left|\frac{1}{r_\mu^3}\right|j\right\rangle \tag{6}$$

(see Fig. 1). The quadrupole radial integral of Eq. (2) is then simply given by

$$W_{E2}^{I'j'Ij}=\langle I'||r^2Y_2||I\rangle\left\langle j'\left|\frac{1}{r_\mu^3}\right|j\right\rangle . \tag{7}$$

In this idealized situation, the nuclear quadrupole matrix element $\langle I'||r^2Y_2||I\rangle$ can be extracted from the hyperfine-splitting energies in a manner that is entirely independent of the shape of the nuclear quadrupole charge density.

However, muonic states that show large $E2$ hyperfine splittings still have appreciable amplitudes inside the nuclear volume. Hence the point nucleus approximation of Eqs. (6) and (7) must be modified to include the effect of the finite size of the charge distribution. We cast Eq. (2) in a form similar to that of Eq. (7),

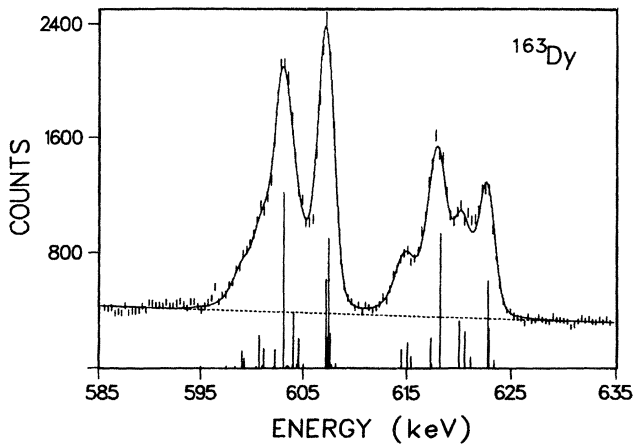

FIG. 6. The muonic M x-ray spectrum of ^{163}Dy. The solid curve represents the best-fit spectrum computed from theory. The vertical lines show the calculated transition energies and intensities. The deduced ground-state quadrupole moment is $Q(\frac{5}{2}^-)=2.648(21)\ e$ b.

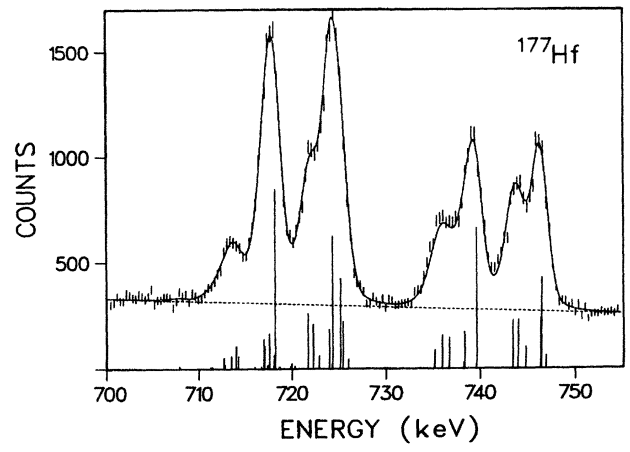

FIG. 8. The muonic M x-ray spectrum of ^{177}Hf. The solid curve represents the best-fit spectrum computed from theory. The vertical lines show the calculated transition energies and intensities. The deduced ground-state quadrupole moment is $Q(\frac{7}{2}^-)=3.365(29)\ e$ b.

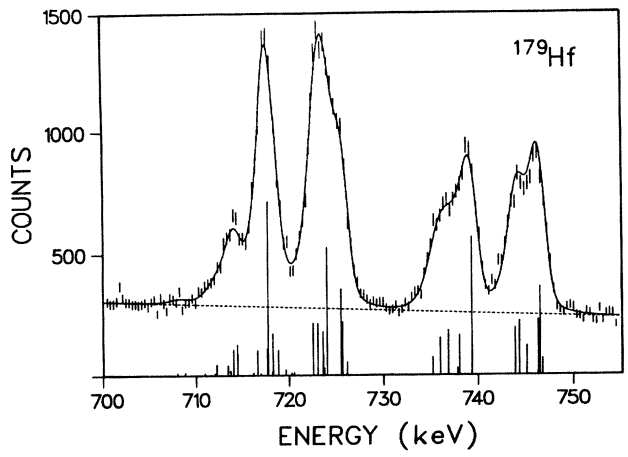

FIG. 9. The muonic M x-ray spectrum of ^{179}Hf. The solid curve represents the best-fit spectrum computed from theory. The vertical lines show the calculated transition energies and intensities. The deduced ground-state quadrupole moment is $Q(\frac{9}{2}^+)=3.793(33)\ e$ b.

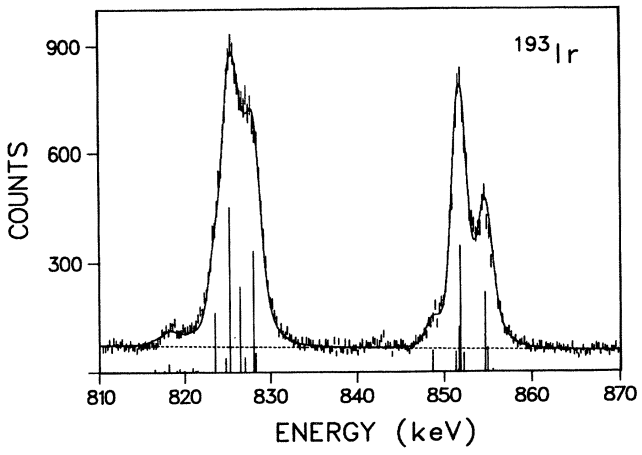

FIG. 11. The muonic M x-ray spectrum of ^{193}Ir. The solid curve represents the best-fit spectrum computed from theory. The vertical lines show the calculated transition energies and intensities. The deduced ground-state quadrupole moment is $Q(\frac{3}{2}^+)=0.751(9)\ e$ b.

$$W_{E2}^{I'j'Ij}=\langle I'||r^2Y_2||I\rangle\frac{\int\rho_{E2}^{I'I}(r)V_{E2}^{j'j}(r)r^2dr}{\int\rho_{E2}^{I'I}(r)r^4dr}\ , \tag{8}$$

where the last factor includes the reduction of the interaction strength due to the finite nuclear charge distribution. If the true charge distribution $\rho_{E2}(r)$ is used, Eq. (8) becomes identical to Eq. (2). However, the true charge density $\rho_{E2}(r)$ is not known and must be approximated, e.g., by Eqs. (3), (5a), and (5b), thus introducing a model error in the value of $\langle I'||r^2Y_2||I\rangle$ deduced from the observed splitting $W_{E2}^{I'j'Ij}$.

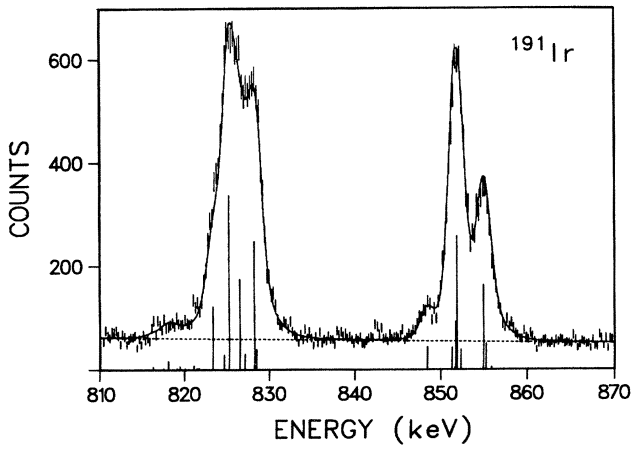

FIG. 10. The muonic M x-ray spectrum of ^{191}Ir. The solid curve represents the best-fit spectrum computed from theory. The vertical lines show the calculated transition energies and intensities. The deduced ground-state quadrupole moment is $Q(\frac{3}{2}^+)=0.816(9)\ e$ b.

The dominant influence on the extracted value of $\langle I'||r^2Y_2||I\rangle$ is the radial position of the peak of $\rho_{E2}^{I'I}(r)$. In order to examine this influence quantitatively, we computed, for various muonic orbitals as a function of Z, the relative change of the extracted $\langle I'||r^2Y_2||I\rangle$ caused by a 10% variation of the quadrupole charge radius R_Q of Eq. (5b). The results, shown in Fig. 2, indicate that for a 10% uncertainty in R_Q, the approximation involved in Eq. (8) introduces a model error in $\langle I'||r^2Y_2||I\rangle$ of less than 1% for a muon in a $2p$ orbit if $Z<20$, for a muon in a $3d$ orbit if $Z<80$, and for a muon in a $4f$ orbit if $Z<100$. The model error is small if the radial dependence of $V_{E2}^{I'j'IJ}(r)$ is close to r^2. This condition is satisfied for all muonic orbits of low Z nuclei and for the outer orbits of high Z nuclei.

It is thus clear that for nuclei in the rare-earth region, quadrupole moments,

$$Q_I=\frac{\sqrt{16\pi}}{\sqrt{5(2I+1)}}(II20\,|\,II)\langle I||r^2Y_2||I\rangle\ , \tag{9}$$

can be determined precisely and nearly model independently from analysis of the hyperfine splittings of muonic $4f\rightarrow 3d$ transitions (M x rays).

III. MEASUREMENTS AND ANALYSES OF MUONIC X-RAY SPECTRA

A. Measurements

The muonic x-ray spectra of the stable isotopes ^{151}Eu, ^{153}Eu, ^{159}Tb, ^{163}Dy, ^{167}Er, ^{177}Hf, ^{179}Hf, ^{191}Ir, and ^{193}Ir were measured at the Los Alamos Meson Physics Facility (LAMPF). The target arrangement, Ge(Li) spectrometer,

TABLE I. Isotopic compositions of targets.

Target	Chemical form	Mass (g)	Isotopic composition (%)				
			151	153			
^{151}Eu	Eu_2O_3	9.67	96.83	3.17			
^{153}Eu	Eu_2O_3	9.88	1.24	98.76			
			159				
^{159}Tb	Tb_2O_3	17.38	99.99				
			162	163	164		
^{163}Dy	Dy_2O_3	18.60	2.67	92.98	3.57		
			166	167	168		
^{167}Er	Er_2O_3	17.90	2.93	91.54	5.14		
			176	177	178	179	180
^{177}Hf	HfO_2	3.97	1.20	86.49	7.47	1.71	3.11
^{179}Hf	HfO_2	2.99	0.18	1.03	3.26	86.98	8.55
			191	193			
^{191}Ir	Ir	9.63	98.17	1.83			
^{193}Ir	Ir	9.95	0.55	99.45			

and data-acquisition system have been described in detail in previous papers.[10,11] The γ rays from ^{24}Na, ^{198}Au, and ^{16}O (Refs. 12 and 13) and the muonic x rays from ^{208}Pb (Refs. 14 and 15) were recorded simultaneously with the data for energy calibration. The energy calibration was based on interpolation of the energies of the γ and x rays of these sources. In separate runs the γ rays from ^{24}Na, ^{56}Co, ^{110}Ag, ^{137}Cs, ^{182}Ta, and ^{16}O were measured to determine the nonlinearity of the data-acquisition system.

The masses, chemical forms, and isotopic compositions of the targets are listed in Table I. We also measured the muonic x rays of the even-A isotopes ^{162}Dy, ^{168}Er, ^{176}Hf, ^{178}Hf, and ^{180}Hf in order to correct for the isotopic impurities in the odd-A targets.

B. Computation of spectra

The nuclear monopole and quadrupole charge densities were constructed from a deformed Fermi charge distribution. The muonic-atom binding energies and eigenfunctions were computed numerically for the various isotopes with the computer program MUON2,[16] which is based on a program written by Rinker.[17] The binding energies were corrected, following Ref. 18, for vacuum-polarization effects, self-energy effects (Lamb shift), electron screening, and relativistic recoil. The corrections also included the effects of the quadrupole vacuum polarization.[19]

With the muonic wave functions so obtained, the matrix elements of the interaction Hamiltonian

$$H_{\mu N}=H(E2)+H(E4)+H(M1)$$

that describe the electric quadrupole, hexadecapole, and magnetic dipole interactions with the relevant nuclear states were computed. The effects of the muonic states that were not included in the model space were taken into account by nuclear polarization corrections. The nuclear polarization energies are small for the muonic $3d$ and higher states, and the errors of the deduced quadrupole moments due to the uncertainties of these correction energies are negligibly small.

C. Analysis of spectra

The muonic x-ray spectra of odd-A deformed nuclei are complex and involve a number of unresolved low-intensity (less than 1%) lines. For this reason, the experimental spectra were directly fitted[20] by theoretical spectra that were constructed by convoluting a theoretical x-ray energy and intensity pattern with the known Ge(Li) detector response function. The detector response was represented by a Gaussian-convoluted Lorentzian with exponential tails. The Lorentzian widths were held fixed at values computed from the natural line widths of the transitions. The exponential tail parameters were determined by fitting the L, M, and N x-ray spectra of ^{208}Pb. Cascade calculations involved in the fitting procedure start from the muonic $5g$ states with the statistical ratio of 8 to 10 for the population of the $5g_{7/2}$ and $5g_{9/2}$ orbits. For each coupled $5g$ muon-nuclear state $|Ij;F\rangle$, we assumed a statistical population proportional to $(2F+1)$.

Figures 3—11 show the muonic M x-ray spectra observed in the present measurements. The solid curve in each figure is the spectrum calculated by the direct spectrum-fitting method described above.[20] The calculated transition energies and intensities are shown by vertical

lines in each figure.

The raw spectra from those targets that contained significant isotopic impurities were corrected by subtracting appropriate fractions of the spectra of the impurity isotopes. Double escape L x-ray lines lie close to the M x-ray lines for muonic atoms with $62 \leq Z \leq 65$. However, these lines are quite weak and can be neglected in the present analysis. Noncircular transitions in this energy region were investigated with the muonic-atom cascade program of Akylas and Vogel,[21] and it was found that the contribution of these lines was also negligible. The quality of the fits, shown in Figs. 3–11, indicates the adequacy of our theoretical representation of the experimental spectra. It also appears that, except for ^{153}Eu, statistical population of the $5g$ hyperfine levels is a good assumption.

D. Intensity anomaly of the hyperfine components in ^{153}Eu

In the ^{153}Eu spectrum, Fig. 4, the observed intensities of the 565- and 563-keV peaks (which involve $|\frac{5}{2}^+ \times 3d_{3/2};3^+\rangle$ and $|\frac{5}{2}^+ \times 3d_{3/2};2^+\rangle$, respectively, as final states) are 10.0(3)% and 9.7(4)%, respectively, while the calculation predicts 11.8% and 8.3%. Also, the observed intensities of the 553-keV peak (which involves $|\frac{5}{2}^+ \times 3d_{5/2};3^+\rangle$ and $|\frac{5}{2}^+ \times 3d_{5/2};4^+\rangle$ as final states) and of the 549-keV peak (which involves the $|\frac{5}{2}^+ \times 3d_{5/2};F\rangle$, $F=0^+$, 1^+, 2^+, and 5^+ states) are 23.9(5)% and 36.2(10)%, while the calculation predicts 25.6% and 34.0%, respectively. The origin of these intensity anomalies in ^{153}Eu is not clear.

The presence of impurity peak(s) of unknown origin embedded in the ^{153}Eu spectrum is unlikely to be responsible for the anomaly, because the experimental ratio of the strengths of the individually summed $3d_{3/2}$ and $3d_{5/2}$ fine structure peaks is quite consistent with the calculation. Inclusion of a simple quadratic term, i.e., $(2F+1)+\epsilon(2F+1)^2$, in the statistical population of the $5g$ levels is not able to explain the data. An arbitrary nonstatistical population of the initial F states, adjusted to fit the observed spectrum, resulted in a quadrupole moment value different by only 0.014 e b. This uncertainty has been added to the statistical error of our listed quadrupole moment for ^{153}Eu. It should perhaps be mentioned that if the same anomaly were to exist in the spectrum of ^{151}Eu, it would add an additional uncertainty of 0.02 e b to the statistical error of our listed quadrupole moment for ^{151}Eu.

IV. QUADRUPOLE MOMENTS AND THEIR UNCERTAINTIES

Table II lists the ground-state quadrupole moments determined in the present experiment, together with the values previously measured[7] for ^{155,157}Gd. The quoted errors in the deduced quadrupole moments include statistical errors, model errors, uncertainties in the effects of low-lying excited nuclear states, and uncertainties of the effects caused by the magnetic and hexadecapole moments of the ground state. (The present analysis is different from that of Ref. 7 for ^{155,157}Gd. For the gadolinium isotopes, the fitted peak energies were compared with the theoretically predicted transition energies, whereas in the present work the entire hyperfine spectrum was fitted directly to the computed spectrum, as discussed earlier. The direct spectrum-fitting method employed here reduces the statistical error from 0.9% to 0.3% for experimental data of comparable quality.)

TABLE II. Measured ground-state quadrupole moments of deformed nuclei.

Nucleus	I^π	Present work Q_I (e b)	Electronic-atom experiment Q_I (e b)
^{151}Eu	$\frac{5}{2}^+$	0.903(10)	1.53(5)[a]
^{153}Eu	$\frac{5}{2}^+$	2.412(21)	3.92(12)[a]
^{155}Gd	$\frac{3}{2}^-$	1.30(2)[b]	1.59(16)[c]
^{157}Gd	$\frac{3}{2}^-$	1.36(2)[b]	1.34(7)[d]
^{159}Tb	$\frac{3}{2}^+$	1.432(8)	1.34(11)[e]
^{163}Dy	$\frac{5}{2}^-$	2.648(21)	2.51(30)[f]
^{167}Er	$\frac{7}{2}^+$	3.565(29)	2.827(12)[g]
^{177}Hf	$\frac{7}{2}^-$	3.365(29)	4.5(5)[h]
^{179}Hf	$\frac{9}{2}^+$	3.793(33)	5.1(5)[h]
^{191}Ir	$\frac{3}{2}^+$	0.816(9)	0.81(21)[i]
^{193}Ir	$\frac{3}{2}^+$	0.751(9)	0.73(19)[i]

[a]Reference 25. Not corrected for the Sternheimer effect.
[b]Reference 7.
[c]P. J. Unsworth, J. Phys. B 2, 122 (1969). Not corrected for the Sternheimer effect.
[d]H.-P. Clieves *et al.*, Z. Phys. A 289, 361 (1979).
[e]W. J. Childs, Phys. Rev. A 2, 316 (1970).
[f]W. J. Childs, Phys. Rev. A 2, 1692 (1970).
[g]K. F. Smith *et al.*, Proc. Phys. Soc. London 86, 1249 (1965). Not corrected for the Sternheimer effect.
[h]S. Buttgenbach *et al.*, Z. Phys. 260, 157 (1973).
[i]S. Buttgenbach *et al.*, Z. Phys. A 286, 333 (1978).

The model error involved in the present M x-ray results was estimated from the effect of a 10% radial displacement of the quadrupole charge radius R_Q of Eq. (5b) with respect to the monopole charge radius, as discussed in Sec. II. The basis of this estimate can be checked by comparing the quadrupole moments deduced from the muonic M x-ray analysis with the quadrupole moments deduced from an analysis of the muonic K and L x rays. In order to extract consistent quadrupole moments from the K and L x-ray analysis, the quadrupole charge radii R_Q had to be reduced by only a few percent from the best fit monopole charge radii (except in ^{151}Eu, where a reduction of almost 10% was necessary). Thus, the model error estimated by the 10% radius change is believed to be generally conservative.

The first and the second excited states of the ground-state rotational band were included in the present analysis. However, the quadrupole moments of these excited states and the $B(E2)$ values between these states and the ground state are not well known for the odd-A nuclei considered here. Hence the $E2$ matrix elements were fixed at the ro-

tational model values calculated (by iteration) from the ground-state quadrupole moments obtained in the present experiment, and an uncertainty of 10% has been assigned to the values of these reduced $E2$ matrix elements. The unknown magnetization distribution in the ground state adds another uncertainty to the deduced quadrupole moment. An error of 10% was assumed for the magnetic hyperfine energy in the muonic $3d$ states. For nuclei with ground-state spins larger than $\frac{3}{2}$, a possible hexadecapole moment of the ground state adds an additional uncertainty to the deduced quadrupole moment. A hexadecapole moment corresponding to a static deformation of $\beta_4=0.0\pm0.1$ was assumed in the calculation. The effects of all these uncertainties are summarized in Table III. The total errors of Q_I are less than 1% for most of the nuclei.

In most cases the present data disagree seriously with the electronic-atom results (see Table II). Such disagreement is perhaps not surprising in view of the difficulty of calculating the electrostatic gradient produced at the nucleus in a multielectron environment, a quantity which is needed to interpret the electronic-atom data. The existence of a nuclear quadrupole moment causes a nonspherical distribution of the core electrons (the Sternheimer effect),[22,23] which in turn affects the valence electronic wave functions. The calculational difficulties are especially pronounced for rare-earth atoms, where the valence electronic wave functions involve a considerable amount of configuration mixing.

In a separate publication[8] we have made a detailed comparison of the present quadrupole-moment values with electronic-atom results. This comparison provides experimental values of the Sternheimer factors for the $4f$, $5d$, and $6p$ electronic states of the rare-earth atoms considered here. The experimental Sternheimer factors are found to vary considerably for different elements and generally are not in agreement with theoretical calculations of the Sternheimer effect. Clearly the theory of the Sternheimer effect needs to be refined before electronic-atom hyperfine experiments can independently give reliable values of nuclear quadrupole moments.

On the other hand, if the appropriate muonic-atom data are available for empirical calibration of the electric field gradient at the nucleus, the electronic-atom measurements can furnish absolute measurements of the quadrupole moments of a wide range of isotopes of the same Z, including very rare or radioactive isotopes.

V. DEFORMATION SYSTEMATICS FOR RARE-EARTH NUCLEI

We have used the present quadrupole moments and those previously determined by the same method,[2–7] together with published $B(E2)$ values from Coulomb excitation experiments on even-A nuclei (Table II of Ref. 24), to investigate the systematics of the quadrupole deformation in rare-earth nuclei. The deformation parameters β_2 were calculated by using the rotational model relationship:

$$\beta_2=\frac{\sqrt{5\pi}}{3ZR_0^2}\frac{(I+1)(2I+3)}{3K^2-I(I+1)}Q_I\ , \tag{10}$$

with $R_0=1.25A^{1/3}$ fm. Figure 12 shows the systematics of the nuclear deformation parameters β_2 for these nuclei.

We first notice the large change of deformation between ^{151}Eu and ^{153}Eu. For this pair of nuclei the change of deformation is larger by more than 50% than for any other pair of nuclei in this region. This observation is consistent with the fact that the largest known isotope shift, $\Delta\langle r^2\rangle=0.577(25)$ fm^2,[25] is observed between the same

TABLE III. Uncertainties involved in the deduced ground-state quadrupole moments.

Nucleus	Statistical error (e b)	Model[a] error (e b)	Dynamic[b] $E2$ hfs (e b)	$M1$ hfs[c] (e b)	$E4$ hfs[d] (e b)	Total error (e b)
^{151}Eu	0.009	0.004	0.002	0.002	0.002	0.010
^{153}Eu	0.017	0.009	0.007	0.001	0.004	0.021
^{159}Tb	0.005	0.006	0.001	0.000		0.008
^{163}Dy	0.010	0.013	0.012	0.001	0.004	0.021
^{167}Er	0.011	0.019	0.019	0.000	0.000	0.029
^{177}Hf	0.009	0.023	0.015	0.000	0.005	0.029
^{179}Hf	0.011	0.026	0.013	0.000	0.011	0.033
^{191}Ir	0.005	0.007	0.002	0.000		0.009
^{193}Ir	0.005	0.007	0.002	0.000		0.009

[a]Model error caused by a 10% change of the quadrupole charge radius R_Q of the transition charge density $\rho_{E2}(r)$ (see Fig. 2).
[b]An uncertainty of 10% was assigned to the reduced $E2$ matrix elements between the low-lying nuclear states.
[c]An uncertainty of 10% was assigned to the magnetic hyperfine energy of the muonic $3d$ states.
[d]An uncertainty due to the hexadecapole moment corresponding to a static deformation $\beta_4=0.0\pm0.1$.

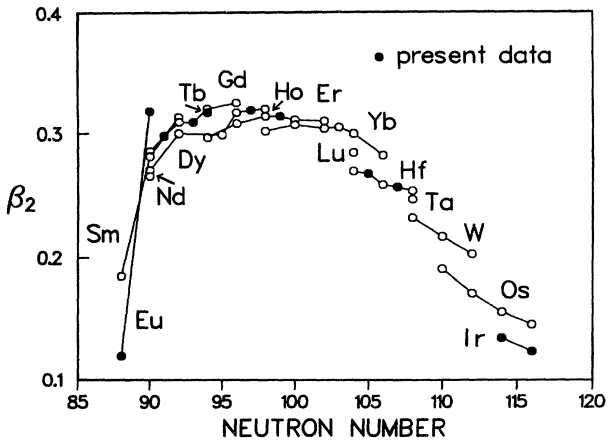

FIG. 12. Systematics of nuclear deformation β_2 for the rare-earth nuclear region. Data are taken from this work, Refs. 2–7, and Table II of Ref. 24.

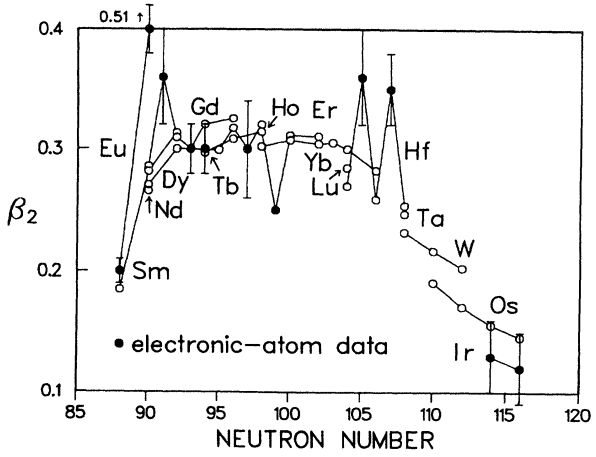

FIG. 13. Systematics of nuclear deformation β_2 for the rare-earth nuclear region based on the latest electronic-atom data as given in the 4th column of Table II. The other data are taken from Refs. 2–7 and Table II of Ref. 24.

pair of nuclei. It is well known that in this region the 89th and 90th neutrons trigger a rather sudden nuclear deformation. In addition, the 63rd proton also seems to have an important role in the change of the nuclear shape, since the deformation difference between $^{151-153}$Eu is much larger than those of $^{150-152}$Sm and $^{152-154}$Gd, and since ^{153}Eu ($Z=63$, $N=90$) exhibits the largest deformation among the $N=90$ isotones.

Except for the nuclei discussed above (which occur at the onset of deformation), the deformation parameters of the odd-A nuclei are entirely consistent in comparison to their adjacent even-A neighbors. In contrast to the results of previous experiments (Fig. 13), both even-A and odd-A nuclei in the mass region $A=150-190$ are now seen to exhibit a very smooth variation of deformation with mass number. In view of the fact that the nuclear deformation is a collective phenomenon,[26,27] it is not surprising that the odd-A valence nucleon plays only a minor role in nuclear deformation.

It has been suggested[28,29] that the odd-even staggering of root-mean-square nuclear charge radii[30,31] may be attributed to a staggering in nuclear deformation between odd and even isotopes. This hypothesis is fairly well supported in the case of gadolinium nuclei,[32] where the change of nuclear deformation between neighboring isotopes is proportional (though with a large uncertainty) to the odd-even staggering of the isotope shifts between these nuclei. However, the odd-even staggering observed in the hafnium nuclei[31,33] is not well explained simply by the change of nuclear deformation.

Because of the difficulty of incorporating an unpaired particle into the theory, odd-A nuclei have not been the subject of Hartree-Fock calculations. Nevertheless, we hope that the availability of precise quadrupole moment values for odd-A nuclei, as presented in this work, will encourage further theoretical work in this field.

VI. SUMMARY

The ground-state quadrupole moments of ^{151}Eu, ^{153}Eu, ^{159}Tb, ^{163}Dy, ^{167}Er, ^{177}Hf, ^{179}Hf, ^{191}Ir, and ^{193}Ir have been determined with an error of about 1% by measuring the quadrupole hyperfine-splitting energies of muonic $4f\rightarrow 3d$ transitions. The model error due to the finite size of the nuclear charge distribution was estimated to be less than 0.4% for nuclei with $A\simeq 150$ and less than 0.9% for nuclei with $A\simeq 190$.

Comparison[8] of the present quadrupole-moment values with electronic-atom results has shown that the theoretical Sternheimer correction factors used in rare-earth electronic-atom analysis are unreliable. However, the present values of nuclear quadrupole moments provide empirical calibration points for electronic-atom experiments, which in turn can yield accurate values for quadrupole moments of a wide range of isotopes of the same element.

Systematics of the deformation parameter β_2 calculated from the present quadrupole moments for odd-A nuclei and from $B(E2)$ values of Coulomb excitation measurements for even-A nuclei indicate that the largest deformation change so far known is found between ^{151}Eu and ^{153}Eu. Except for ^{151,153}Eu, the deformation parameters of the other odd-A nuclei show a very smooth variation of deformations with respect to the adjacent even-A nuclei.

It has been suggested that the odd-even staggering of isotope shifts is due to a staggering of nuclear deformation between odd and even isotopes. However, the present quadrupole-moment values indicate, though with a large uncertainty, that the odd-even staggering phenomenon is not satisfactorily explained by the deformation effect alone.

ACKNOWLEDGMENTS

The authors wish to thank R. A. Naumann for fruitful discussions. This work was supported by the U.S. Department of Energy. All work was carried out at Los Alamos National Laboratory. One of the authors (W.R.) was supported in part by the Deutscher Akademischer Austauschdienst, Bonn, Federal Republic of Germany.

[1]H. J. Leisi, W. Dey, P. Ebersold, R. Engfer, F. Scheck, and H. K. Walter, J. Phys. Soc. Jpn. 34, Suppl. 355 (1973).
[2]W. Dey, P. Ebersold, H. J. Leisi, F. Scheck, H. K. Walter, and A. Zehnder, Nucl. Phys. A326, 418 (1979).
[3]A. Zehnder, F. Boehm, W. Dey, R. Engfer, H. K. Walter, and J.-L. Vuilleumier, Nucl. Phys. A254, 315 (1975).
[4]R. J. Powers, F. Boehm, P. Vogel, A. Zehnder, T. King, A. R. Kunselman, P. Roberson, P. Martin, G. H. Miller, R. E. Welsh, and D. A. Jenkins, Nucl. Phys. A262, 493 (1976).
[5]R. J. Powers, F. Boehm, A. Zehnder, A. R. Kunselman, and P. Roberson, Nucl. Phys. A278, 477 (1977).
[6]R. J. Powers, F. Boehm, A. A. Hahn, J. P. Miller, J.-L. Vuilleumier, K.-C. Wang, A. Zehnder, A. R. Kunselman, and P. Roberson, Nucl. Phys. A292, 487 (1977).
[7]Y. Tanaka, D. B. Laubacher, R. M. Steffen, E. B. Shera, H. D. Wohlfahrt, and M. V. Hoehn, Phys. Lett. 108B, 8 (1982).
[8]Y. Tanaka, R. M. Steffen, E. B. Shera, W. Reuter, M. V. Hoehn, and J. D. Zumbro, Phys. Rev. Lett. 51, 1633 (1983).
[9]L. K. Wagner, E. B. Shera, G. A. Rinker, and R. K. Sheline, Phys. Rev. C 16, 1549 (1977).
[10]E. B. Shera, E. T. Ritter, R. B. Perkins, G. A. Rinker, L. K. Wagner, H. D. Wohlfahrt, G. Fricke, and R. M. Steffen, Phys. Rev. C 14, 731 (1976).
[11]Y. Yamazaki, E. B. Shera, M. V. Hoehn, and R. M. Steffen, Phys. Rev. C 18, 1474 (1978).
[12]R. C. Greenwood, R. G. Helmer, and R. J. Gehrke, Nucl. Instrum. Methods 159, 465 (1979).
[13]E. B. Shera, Phys. Rev. C 26, 2321 (1982).
[14]L. Tauscher, G. Backenstoss, K. Fransson, H. Koch, A. Nilsson, and J. De Raedt, Z. Phys. A 285, 139 (1978).
[15]M. V. Hoehn and E. B. Shera (unpublished).
[16]Y. Tanaka, programs MUON2 and XRAY2 (unpublished).
[17]G. A. Rinker, Comput. Phys. Commun. 16, 221 (1979).
[18]G. A. Rinker and R. M. Steffen, At. Data Nucl. Data Tables 20, 143 (1977).
[19]J. M. McKinley (unpublished). An explicit form of this correction can be found in Ref. 3.
[20]E. B. Shera, program XRAY3 (unpublished).
[21]V. R. Akylas and P. Vogel, Comput. Phys. Commun. 15, 291 (1978).
[22]R. M. Sternheimer, Phys. Rev. 146, 140 (1966); 164, 10 (1967).
[23]R. M. Sternheimer and R. F. Peierls, Phys. Rev. A 3, 837 (1971).
[24]R. M. Ronningen, J. H. Hamilton, L. Varnell, J. Lange, A. V. Ramayya, G. Garcia-Bermudez, W. Lourens, L. L. Riedinger, F. K. McGowan, P. H. Stelson, R. L. Robinson, and J. L. C. Ford, Jr., Phys. Rev. C 16, 2208 (1977).
[25]H. Brand, V. Pfeufer, and A. Steudel, Z. Phys. A 302, 291 (1981).
[26]A. Bohr, K. Dan. Vidensk. Selsk. Mat.-Fys. Medd. 26, No. 14 (1952).
[27]K. Kumar and M. Baranger, Nucl. Phys. A110, 529 (1968).
[28]L. Wilets, D. L. Hill, and K. W. Ford, Phys. Rev. 91, 1488 (1953).
[29]B. S. Reehal and R. A. Sorensen, Nucl. Phys. A161, 385 (1971).
[30]R. Engfer, H. Schneuwly, J.-L. Vuilleumier, H. K. Walter, and A. Zehnder, At. Data Nucl. Data Tables 14, 509 (1974).
[31]K. Heilig and A. Steudel, At. Data Nucl. Data Tables 14, 613 (1974).
[32]D. B. Laubacher, Y. Tanaka, R. M. Steffen, E. B. Shera, and M. V. Hoehn, Phys. Rev. C 27, 1772 (1983).
[33]Y. Tanaka, R. M. Steffen, E. B. Shera, W. Reuter, M. V. Hoehn, and J. D. Zumbro (unpublished).